

Automated Tracing of the Adventitial Contour of Aortoiliac and Peripheral Arterial Walls in CT Angiography (CTA) to Allow Calculation of Non-calcified Plaque Burden

Bhargav Raman · Raghav Raman · Geoffrey D. Rubin · Sandy Napel

Published online: 10 March 2011
© Society for Imaging Informatics in Medicine 2011

Abstract Aortoiliac and lower extremity arterial atherosclerotic plaque burden is a risk factor for the development of visceral and peripheral ischemic and aneurismal vascular disease. While prior research allows automated quantification of calcified plaque in these body regions using CT angiograms, no automated method exists to quantify soft plaque. We developed an automatic algorithm that defines the outer wall contour and wall thickness of vessels to quantify non-calcified plaque in CT angiograms of the chest, abdomen, pelvis, and lower extremities. The algorithm encodes the search space as a constrained graph and calculates the outer wall contour by deriving a minimum cost path through the graph, following the visible outer wall contour while minimizing path tortuosity. Our algorithm was statistically equivalent to a reference standard made by two reviewers. Absolute error was $1.9 \pm 2.3\%$ compared to the inter-observer variability of $3.9 \pm 3.6\%$. Wall thickness in vessels with atherosclerosis was 3.4 ± 1.6 mm compared to 1.2 ± 0.4 mm in normal vessels. The algorithm shows promise as a tool for quantification of non-calcified plaque in CT angiography. When combined with previous research, our method has the potential to quantify both non-calcified and calcified plaque in all clinically significant systemic arteries, from the thoracic aorta to the arteries of the calf, over a wide range of diameters. This algorithm has the potential to enable risk stratification of patients and facilitate investigations into the relationships between asymptomatic atherosclerosis and a variety of behavioral, physiologic, pathologic, and genotypic conditions.

Keywords Soft plaque · Quantification · Algorithm · CT angiography · Arteries · Graph method

Background

Aortoiliac and lower extremity arterial atherosclerosis is a risk factor for the development of visceral and peripheral ischemic and aneurismal vascular disease [1–5]. CT angiograms are the standard for noninvasive evaluation of systemic atherosclerotic disease [6–8].

The speed and coverage of multi-detector row CT (MDCT) allows the imaging of the aortoiliac system in a single scan, presenting a unique opportunity to quantify the atherosclerotic burden subdivided into calcified and non-calcified components. Overall atherosclerotic plaque burden is an independent risk factor for the development and severity of coronary artery disease [9]. In contrast, risk factors such as hyperlipidemia and obesity do not accurately predict coronary plaque burden, and these same risk factors are only variably associated with systemic atherosclerotic burden [10]. Coronary CT angiography (CTA) is not currently recommended as a screening test and a special protocol must be used for image acquisition, whereas contrast-enhanced MDCT of the chest and/or of the abdomen and pelvis is conducted for a variety of different indications. Determining the quantity and distribution of plaque in the arterial system in these scans potentially allows risk stratification of patients for both coronary and extra-coronary vascular disease to be performed. Furthermore, determining the quantity and distribution of plaque throughout the arterial system would facilitate investigations into the relationships between asymptomatic atherosclerosis and a variety of behavioral, physiologic, pathologic, and genotypic conditions.

B. Raman (✉) · R. Raman · G. D. Rubin · S. Napel
Department of Radiology,
Stanford University School of Medicine,
Stanford, CA 94305-5105, USA
e-mail: ramanb@stanford.edu

Previous methods of automated quantification of the severity and distribution of atherosclerosis have detected and quantified mural calcification as a marker for atherosclerotic plaque [11]. While calcium is highly correlated with atherosclerotic burden [12], the quantification of all plaque, both calcified and non-calcified, may yield a more accurate measure.

Because non-calcified plaque has a density similar to soft tissue, it is difficult to quantify. Non-calcified plaque quantification using CT has been reported in the coronary arteries [13–16]. Since the majority of the coronary arteries course within a layer of fat, a consistent contrast difference between vessel wall and surrounding fat exists in many regions and makes it easier to quantify and characterize coronary plaques. However, in extra-coronary arteries, the outer contour is harder to delineate. In some regions, there is adequate contrast between the outer vessel wall (which measures 0–50 HU) and its surroundings (e.g., fat (measuring less than –20 HU) or aerated lung). However, in many other regions, the vessel wall is closely opposed to other soft tissue structures such as muscle, bowel wall, etc., with a very thin layer of fat interposed. Due to volume averaging, this thin layer of fat can have artifactually higher HU values, further reducing the available contrast. In the retroperitoneum, the vessel wall may be adjacent to other structures, such as the inferior vena cava, with no apparent intervening fat. Similarly, in the lower extremities, close opposition between the outer wall of the artery and muscle or soft tissue reduces contrast. In these and other regions, there may be no density difference or gradient that can be used to identify and follow the outer contour of the vessel. Manual methods of tracing the outer contour are time-consuming and imprecise.

Our purpose was to develop an algorithm that defines the outer contour of the wall of systemic arteries to allow quantification of non-calcified plaque burden and to evaluate its use in CTA scans of the chest, abdomen, pelvis, and lower extremities.

Material and Methods

Our algorithm requires the user to first select a point in the aortic lumen near the superior extent of the scan and at the end of each artery of interest. A previously developed algorithm [17, 18] is then applied to derive a 3D branched median centerline between the point in the aortic lumen and all defined endpoints. From the median centerline, cross-sections perpendicular to the aortic lumen are obtained at 1-mm intervals. Then, for each perpendicular cross-section, three steps are performed: (1) The inner wall contour is calculated, (2) a search space for the outer contour is defined, and (3) the space is encoded as a graph with nodes and edge weights and the final outer contour is derived by

calculating the minimum cost path through the graph. Each of these steps is discussed in detail below.

Inner Wall Contour

From the centerlines, we define the volume occupied by the arterial lumen while excluding other vessels and surrounding soft tissue. To accomplish this, a list of centerline points is obtained by sampling the median centerlines at sub-voxel intervals. The perpendicular luminal cross-section through each of these points is then segmented using the point as a seed for region growing based upon an adaptive threshold computed from the voxel intensity statistics near the seed point. The average size and shape of the previous five segmentations are used to constrain the subsequent segmentation from extending into adjacent veins or arterial branches. The circumference of each segmented cross-section is stored as the inner (luminal) contour, and the collection of all such cross-sections defines the luminal volume.

Search Space

The search space is defined on each cross-section as a 10-mm-wide strip parallel to the inner wall contour. This search space is assumed to contain the outer wall contour and was chosen because it was unlikely that the vessel wall would be thicker than 10 mm, except in regions with aneurysmal atherosclerotic disease. Since the algorithm was not intended to quantify wall thickness in the presence of thrombus lining the lumina of aneurysms, it was felt that limiting the search space to 10 mm was reasonable.

We define a set of nodes within this search space using a polar coordinate system with respect to the center of the vessel. Accordingly, each node is assigned two values, r and θ , where r represents the distance of the node from the center of the vessel and θ represents the angular position of the node with respect to the up direction of the perpendicular cross-section. These nodes were defined such that each node was separated by 1° in the circumferential direction and 0.5 mm in the radial direction (Fig. 1).

Graph Encoding

The algorithm then encodes the search space as a graph with directional edges connecting the nodes. Edges are only defined between voxels whose difference in θ is $+1^\circ$. This creates a graph whose edges are constrained to extend circumferentially around the vessel. Edge weights (EW) are calculated from two terms, an intensity weight (IW) and a distance weight (DW). The intensity weight is calculated such that the lowest cost is associated with voxels at the periphery of the outer wall of the vessel, which are typically around 0 HU in intensity since they contain both fat and

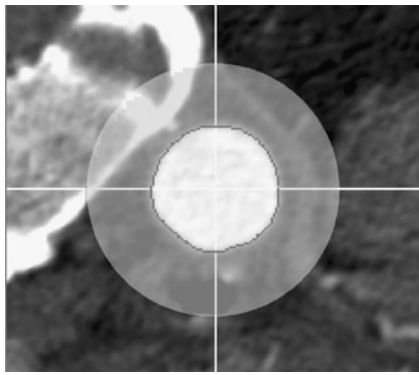


Fig. 1 CT section of the abdominal aorta showing inner wall (black) and search area (light white). Crosshairs represent the location of the median centerline

soft tissues. To favor these voxels, the transfer function is defined in the following manner.

Each voxel is assigned an IW of between 0 and 1. Voxels that have an intensity of <0 HU (water intensity) are assigned an IW of 0. The noise in the scan is calculated using the root mean squared error, hereby referred to as σ . Voxels with HU intensities above $2*\sigma$ are assigned an IW of 1. The IW assigned to each voxel between 0 HU and $2*\sigma$ HU is based on the following equation:

$$IW = \cos(HU/(2*\sigma))$$

The DW is used to favor paths that are shorter or less tortuous and is defined as the Euclidean distance between nodes in millimeters.

The final transfer function is then expressed as:

$$EW = IW + \alpha \times DW,$$

where α encodes the relative importance of the distance weight. Given the above graph encoding, a standard shortest path algorithm (Bellman–Ford) is then used to calculate the minimum cost path through the graph from $\theta=0^\circ$ to $\theta=359^\circ$

Optimization of α

To determine an optimal value for α , we retrospectively obtained five consecutive CTAs of the chest, abdomen, pelvis, and lower extremity from patients (four men, one woman; age, 36–79 years) with a clinical history of vascular disease but no evidence of aneurismal vascular disease (abdominal aortic diameter <3 cm or thoracic aortic diameter <4 cm) and five consecutive CTAs from patients (three women, two men; age, 19–86 years) without clinical history of vascular disease who underwent CTA for other clinical indications. These ten scans were acquired at 120 kV, 350–440 mA, 0.6- to 0.8-mm reconstruction interval, and 1- to 1.25-mm slice thickness and were obtained under our institution's IRB for retrospective

studies and de-identified before processing in compliance with HIPAA requirements. Five vascular regions were defined: (a) thoracic aorta, (b) abdominal aorta, (c) common iliac artery, (d) external iliac/common femoral arteries, and (e) superficial femoral/popliteal/anterior tibial arteries. For each region, ten sections perpendicular to the course of the artery were randomly chosen in each patient, for a total of 500 sections. The reference standard for the outer wall locations were outlined on all selected sections by one of the authors.

Over all slices, the value of α was varied between 1 and 2,000, with intervals of 10, and the mean error in millimeters between the computed outer wall and the reference standard outer wall was recorded. The value of α that yielded the lowest error across all scans was chosen as the optimized value. Subsequently, sensitivity analysis was carried out for the variable α as follows. For the ten scans, the values for α that were optimal for each scan were collected. The 10th percentile optimal value for α and the 90th percentile optimal value for α for this set of ten scans were identified. These two values were used to compute two sets of outer wall contours for each of the ten scans. The errors for these two values of alpha were compared to quantify the dependence of outer wall contour computation on α .

Validation

To evaluate the algorithm, we retrospectively obtained, starting from 28 January 2008, 20 consecutive CTA scans from patients (12 of the chest, abdomen, and pelvis (average dose, 14.4 mSv) and 8 of the abdomen, pelvis, and lower extremities (average dose, 15.1 mSv); 12 men, 8 women; age, 26–87 years) with no evidence of aneurismal vascular disease (abdominal aortic diameter <3 cm or thoracic aortic diameter <4 cm). The scans were obtained without regard to history of other vascular disease. Scans were acquired at 120 kV, 380–517 mA, 0.6- to 0.8-mm reconstruction interval, and 1- to 1.25-mm slice thickness and were obtained under our institution's IRB for retrospective studies and de-identified before processing in compliance with HIPAA requirements. Between 80- and 120-mL Isovue (300 or 370) iodinated contrast was used for vessel enhancement (Bracco Diagnostics Inc. Princeton, NJ). This produced a luminal enhancement of 130–300 HU in the test scans. All scans were distinct from those used to optimize α .

Cross-sections perpendicular to the lumen of the arteries in the five vascular regions previously described were obtained. Images were categorized by vascular region and by whether they had or had no atherosclerotic plaque (ten categories). Of the images in each category, eight were randomly selected to yield a total of 80 images. Two experienced 3D technologists (reviewers) then traced the

outer wall on all images. The outer wall traces were then quantized using polar coordinates with one radius value per degree. The traces were then averaged to generate a reference standard. To calculate inter-observer variability, the absolute difference of the radius value was calculated for each degree between the two reviewers' traces. These absolute values were averaged to calculate the average absolute error for the two reviewers' traces being compared. The absolute error between the automated trace and the reference standard was calculated in a similar way. The inter-observer variability was then compared to the error between the automated method and the reference standard contours. Results were analyzed over all vascular regions and for each vascular region separately.

The maximum measured arterial wall thickness measured in each image was calculated. The maximum wall thickness in the 40 images without atherosclerotic plaque was compared to the maximum measured arterial wall thickness in the 40 images with atherosclerotic plaques to evaluate whether our algorithm was able to show an increase in wall thickness in the presence of atherosclerotic plaque.

The time to create the reference standards was compared to the algorithm's run time. Operator time required to define a start and end points for the algorithm was only a few seconds and therefore was not considered in the statistics.

Statistics

Schuirmann's paired two one-sided equivalence tests [19] were used to test the null hypothesis that the radii of the reference standard were different from those produced by the algorithm and the null hypothesis that the radii of one reviewer were different from the other reviewer. Concordance correlations between the reference standard and the algorithm were also obtained, as well as correlations between the two reviewers. The above tests were also calculated for each vascular region separately. The maximum wall thickness in images without atherosclerotic plaque was compared to the maximum wall thickness in images with atherosclerotic plaques using an unpaired *t* test. Time to create reference standards was compared to the algorithm's run time using a paired *t* test.

Results

Optimization of α

Table 1 reports the optimal values of α , radial errors obtained at the overall optimal, and the 10th and 90th percentile values for α for each of the ten scans that were obtained solely for this purpose. The mean optimal value

for α was 554 ± 184 (SD). When this value was used for α , radii measured using the automated algorithm had an error (mean \pm SD) of $1.7 \pm 1.1\%$ compared to the reference standard. The 10th and 90th percentile values for α were 394 and 723, respectively. When the 10th percentile value for α (394) was used, radii measured using the automated algorithm had an error (mean \pm SD) of $2.1 \pm 2.2\%$ compared to the reference standard. When the 90th percentile value for α (723) was used, radii measured using the automated algorithm had an error (mean \pm SD) of $2.4 \pm 2.5\%$ when compared to the reference standard. In this sensitivity analysis, a change in α of 60% from the optimal value of 550 resulted in a mean increase in the error over all ten scans of 0.7% (maximum of $2.4 \pm 1.3\%$ increase in error in each scan).

Comparison to Reviewers

For the 80 cross-sectional images obtained from the 20 scans, our method was able to produce outer wall boundaries in all images. Figure 2 shows examples of the outer wall boundaries calculated by the automated method in each vascular region. Outer wall radii derived from the boundaries ranged from 2.0 to 29.0 mm. Table 2 shows the measured error, the inter-observer variability, the results of Schuirmann's test, the result of the concordance correlation between the algorithm and the reviewers, and the result of the concordance correlation between reviewers for each region separately. Compared to the reference standard, radii measured using the automated algorithm had an error (mean \pm SD) of $1.9 \pm 2.3\%$. In comparison, the difference between reviewers was $3.9 \pm 3.6\%$. There was no statistically significant difference between the radii measured using the algorithm versus those of the reference standard (Schuirmann's paired two one-sided equivalence test, $p < 0.05$). The overall concordance correlation between the algorithm and the reviewers was 0.99. The overall concordance correlation between reviewers was 0.99. Although not statistically significant, an upward trend is noted in absolute error and in inter-observer variability in smaller arteries compared to the manually drawn standard. This trend was not noted with concordance correlations and the algorithm was statistically equivalent to manually drawn standards in all regions (Schuirmann's paired two one-sided equivalence tests, $p < 0.05$).

Comparison Between Images

with and Without Atherosclerotic Plaques

The measured maximal wall thickness in images without and with atherosclerotic plaques was 1.2 ± 0.4 and 3.4 ± 1.6 mm, respectively. These were significantly different (unpaired *t* test, $p < 0.01$).

Table 1 Error with respect to gold standard using various alpha constants

| Scan | Optimal alpha | Error (%), $\alpha=554$ | Error (%), $\alpha=394$ (10th percentile) | Error (%), $\alpha=723$ (90th percentile) | Maximum increase in error (%) |
|------|---------------|-------------------------|---|---|-------------------------------|
| 1 | 240 | 3.9 | 0.3 | 6.5 | 3.6 |
| 2 | 410 | 2.2 | 0.2 | 6.1 | 3.9 |
| 3 | 420 | 1.1 | 0.5 | 1.2 | 0.6 |
| 4 | 430 | 1.7 | 0.3 | 5.3 | 3.5 |
| 5 | 500 | 0.4 | 1.0 | 1.0 | 0.6 |
| 6 | 600 | 1.6 | 2.0 | 1.8 | 0.4 |
| 7 | 690 | 0.2 | 1.3 | 0.9 | 1.1 |
| 8 | 700 | 2.1 | 5.2 | 0.4 | 3.1 |
| 9 | 710 | 1.0 | 4.4 | 0.4 | 3.4 |
| 10 | 840 | 2.8 | 5.8 | 0.4 | 3.1 |
| Mean | | 1.7±1.1 | 2.1±2.2 | 2.4±2.5 | 2.4±1.3 |

Time

Reviewers required 66 ± 42 s (SD) per image to define the outer and inner contours, while the algorithm required 0.04 ± 0.02 s (SD) per image. These were significantly different (paired *t* test, $p<0.01$).

Discussion

Although measurement of calcification using CT is commonly used as a measure of atherosclerosis, non-calcified plaque quantification has been mainly limited to ultrasound and MRI

because of the higher contrast resolution allowing better visualization of soft tissue [20–47]. However, the carotid and coronary arteries are smaller vascular beds, whereas quantification of systemic atherosclerosis requires a much larger scan range, especially if the lower extremities are included, to assess risk for peripheral artery disease. Ultrasound is necessarily a local imaging tool, and a whole body MRI may not give sufficient resolution for effective quantification within a reasonable scan time. Calcification is also better visualized and quantified on CT. Although detection of non-calcified plaque has been explored using computed tomography [6, 13, 16], no automated quantitative method has yet been developed for this modality. One method proposed by

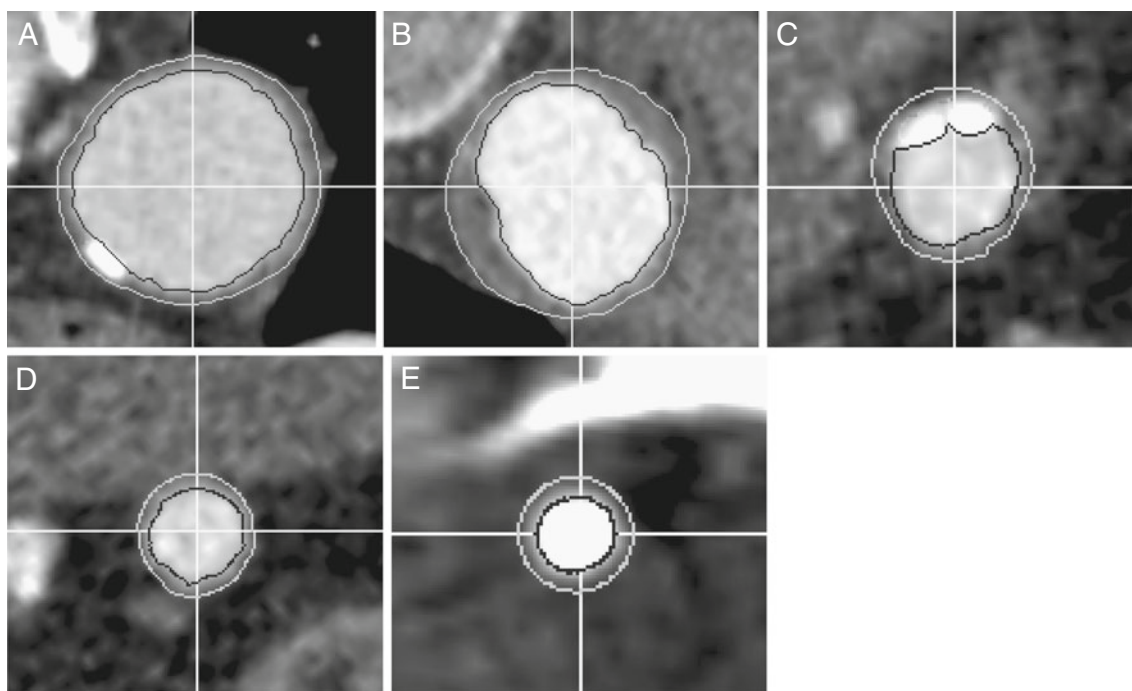


Fig. 2 CT sections, from different patients, of the thoracic aorta (a), abdominal aorta (b), common iliac artery (c), external iliac artery (d), and popliteal artery (e), perpendicular to the median luminal

centerline, showing inner wall (black line) and final calculated outer wall (white line). Crosshairs represent the location of the median centerline

Table 2 Measured error and inter-observer variability in each vascular region

| Region (average radius, mm) | Measured error, mm (%) | Inter-observer variability, mm (%) | Schuirmann's test of equivalence (<i>p</i> value) | Concordance correlation, algorithm versus reviewers | Concordance correlation, between reviewers |
|--|---------------------------|---------------------------------------|--|---|--|
| Thoracic aorta (14.8±0.71) | 0.24±0.17 (1.65±1.17) | 0.51±0.40 (3.45±2.72) | <0.05 | 0.912 | 0.658 |
| Abdominal aorta (14.8±0.93) | 0.22±0.16 (1.52±1.10) | 0.41±0.33 (2.81±2.3) | <0.05 | 0.993 | 0.985 |
| Common iliac artery (7.00±0.54) | 0.15±0.15 (2.11±2.22) | 0.28±0.23 (3.93±3.02) | <0.05 | 0.928 | 0.798 |
| External iliac and common femoral arteries (5.52±0.68) | 0.16±0.11 (2.91±2.19) | 0.24±0.19 (4.43±3.65) | <0.05 | 0.960 | 0.906 |
| Superficial femoral, popliteal, anterior tibial arteries (3.94±0.47) | 0.12±0.11 (3.12±3.4) | 0.18±0.18 (4.74±5.35) | <0.05 | 0.944 | 0.848 |
| Overall | 0.15±0.15 (1.89±2.27) | 0.32±0.30 (3.88±3.63) | <0.05 | 0.998 | 0.995 |

Shum et al. [48] quantifies wall thickness in the presence of thrombus in abdominal aortic aneurysms. This method relies on a median filter edge detector and extensive manual interaction to set thresholds for the detection of the outer wall. The paper is mainly concerned with the detection of the inner wall, which is obscured by intraluminal thrombus. The

algorithm applies only to abdominal aortic aneurysms with intraluminal thrombus, whereas our algorithm is designed to calculate wall thickness in all clinically significant arteries in patients without severe vascular disease. When combined with previous research [11], our method has the potential to quantify both non-calcified and calcified plaques in all

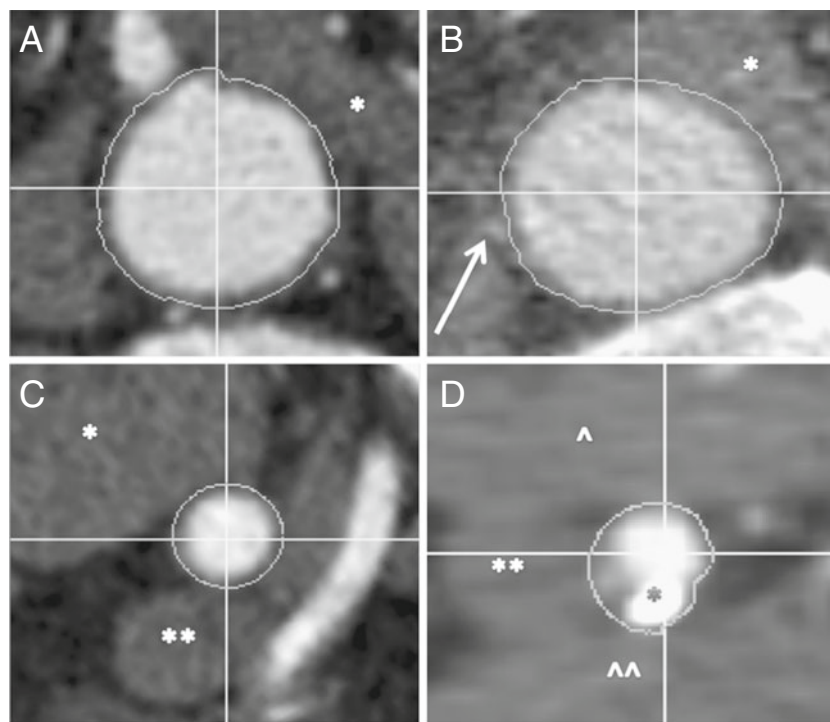


Fig. 3 Oblique reformats perpendicular to the course of the artery showing examples of algorithm performance when the outer wall border is obscured by adjacent soft tissues. The white outline represents the outer wall contour calculated by the algorithm. Crosshairs represent the location of the median centerline. **a** Abdominal aorta just distal to celiac axis origin. Crura of the diaphragm obscures outer wall of aorta anterolaterally (*asterisk*). **b** Distal descending thoracic aorta. The crus of the diaphragm obscures most of outer wall of the aorta anteriorly (*asterisk*). Adjacent bone obscures the outer wall posteriorly. An

adjacent lumbar artery (*arrow*) could be mistaken for a mural calcification on this image, but the algorithm correctly excludes it. **c** Right external iliac artery. Psoas muscle obscures the outer wall anteriorly (*asterisk*), and the bifurcation of the common iliac vein obscures the outer wall posteriorly (*two asterisks*). **d** Left superficial femoral artery. Calculated outer wall contour correctly includes focal mural atherosclerotic calcification (*asterisk*). Superficial femoral vein obscures outer wall laterally (*two asterisks*), vastus medialis obscures outer wall anteriorly (*circumflex*), and semimembranosus muscle obscures outer wall posteriorly (*two circumflex symbols*)

clinically significant systemic arteries, from the thoracic aorta to the arteries of the calf, over a wide range of diameters.

Automated and semi-automated *in vivo* methods of quantifying aortic wall thickness have been studied before using both MRI and transdermal and intravascular ultrasound [20, 21, 23, 24, 26, 28, 38, 42, 45]. More detailed characterization of individual plaques by MRI has also been validated against pathological specimens [24]. However, characterization by both MRI and ultrasound has been largely limited to individual plaques or smaller vascular beds such as the carotid or the coronary arteries, and there is no existing literature describing a method for global characterization of systemic plaque burden that includes the lower extremity arteries. One prior method reported by Adame et al. [20] relied heavily on detecting periaortic fat using axial MRI slices and an ellipse fitting procedure to calculate the outer wall contour. Although the method has excellent correlation with manual measurement, this method does not take into account artery orientation, which is important in smaller arteries and older patients with more tortuous large arteries. The method also requires an MRI sequence that is not currently in clinical practice, assumes that the wall is almost circular, and assumes that the outer wall is largely parallel to the inner wall. Our method is independent of artery orientation and uses a standard CT angiography protocol that is routinely used for other indications.

Adjacent soft tissue or vascular structures that abut the outer wall of a blood vessel pose the greatest challenge for vascular segmentation, even for experienced human reviewers. Common adjacent structures include the diaphragmatic crura, bowel, bone, musculature, and other arteries and veins. Our algorithm, by its nature, follows the unobscured wall closely and uses a tuned weighting factor to follow the obscured outer wall with accuracy similar to human observers in a variety of vascular beds and adjacent soft tissue structures, as exemplified in Fig. 3.

The precision of our algorithm could be affected by differences in user selection of the arterial points. While we did not assess this directly, these user inputs only affect the location of the centerline used to create orthogonal cross-sections. In a previous study [49], it was shown that the centerline algorithm that we use was highly insensitive to these inputs, and so we expect our results to be similarly precise.

The results of the sensitivity analysis (Table 1) indicate that errors in thickness measurement are insensitive to choice of the distance weight, α , over a large range of α . This indicates that a single optimal value of α can be calculated from a representative set of scans. Also, since our algorithm is deterministic, the outer wall contour that is calculated is guaranteed to be the one that conforms to the global minimum cost.

Our algorithm was designed to reduce user interaction time to a few seconds and achieves an average time of 0.04 s per image, enabling quantification of a scan of the whole body in about 1 min, which makes automated quantification clinically viable. One important factor reducing processing time is that edges of the graph are constrained to a course around the circumference of the vessel. Thereby, the number of possible paths is reduced.

While there is no imaging gold standard with which to assess accuracy, our method gives results that are within the range of human precision. Validation with manual determination on 20 CT angiograms showed that the measured error of the automated algorithm was comparable to the inter-observer variability. Although the error does increase (though not significantly) with smaller arteries, it is still within the range of human variation. The measured maximum wall thickness in images with atherosclerotic plaque is significantly greater than the maximum wall thickness in images without atherosclerotic plaques, indicating that the algorithm has potential to be used for detecting and quantifying atherosclerotic regions of the arterial wall.

Conclusion

Our algorithm allows the outer contour of the vessel to be calculated precisely with accuracy that is not significantly different compared to manual methods, allowing calculation of vessel wall thickness as a measure of non-calcified plaque burden.

References

1. Wassef M, Upchurch Jr, GR, Kuivaniemi H, Thompson RW, Tilson 3rd, MD: Challenges and opportunities in abdominal aortic aneurysm research. *J Vasc Surg* 45:192–198, 2007
2. Allison MA, Kwan K, DiTomasso D, Wright CM, Criqui MH: The epidemiology of abdominal aortic diameter. *J Vasc Surg* 48:121–127, 2008
3. Ito S, et al: Differences in atherosclerotic profiles between patients with thoracic and abdominal aortic aneurysms. *Am J Cardiol* 101:696–699, 2008
4. Fagan-Dubin L: Atherosclerosis: a major cause of peripheral vascular disease. *Nurs Clin North Am* 12:101–108, 1977
5. Lee AJ, Fowkes FG, Carson MN, Leng GC, Allan PL: Smoking, atherosclerosis and risk of abdominal aortic aneurysm. *Eur Heart J* 18:671–676, 1997
6. Sassa S, Shimada K, Yoshida K, Tanaka H, Jissho S, Yoshikawa J: Comparison of 64-slice multi-detector computed tomography coronary angiography between asymptomatic, type 2 diabetes mellitus and impaired glucose tolerance patients. *J Cardiol* 52:133–139, 2008
7. Napoli A, et al: 64-MDCT imaging of the coronary arteries and systemic arterial vascular tree in a single examination: optimisation of the scan protocol and contrast-agent administration. *Radiol Med* 113:799–816, 2008

8. Takasu J, et al: Inflammation and descending thoracic aortic calcification as detected by computed tomography: the multi-ethnic study of atherosclerosis. *Atherosclerosis* 199:201–206, 2008
9. Yorgun H, Hazirolan T, Kaya EB, et al: Aortic atherosclerosis predicts the extent and severity of coronary atherosclerosis detected by multidetector computed tomography coronary angiography. *Angiology* 61:627–632, 2010
10. Johnson KM, Dowe DA, Brink JA: Traditional clinical risk assessment tools do not accurately predict coronary atherosclerotic plaque burden: a CT angiography study. *AJR Am J Roentgenol* 192:235–243, 2009
11. Raman R, Raman B, Napel S, Rubin GD: Semiautomated quantification of the mass and distribution of vascular calcification with multidetector CT: method and evaluation. *Radiology* 247:241–250, 2008
12. Sangiorgi G, et al: Arterial calcification and not lumen stenosis is highly correlated with atherosclerotic plaque burden in humans: a histologic study of 723 coronary artery segments using non-decalcifying methodology. *J Am Coll Cardiol* 31:126–133, 1998
13. Sun J, et al: Identification and quantification of coronary atherosclerotic plaques: a comparison of 64-MDCT and intravascular ultrasound. *AJR Am J Roentgenol* 190:748–754, 2008
14. Shakeri AB, Tubbs RS, Shoja MM, Ghabili K, Rahimi-Ardabili B, Loukas M: Screening for thoracoabdominal aortic aneurysms in patients with aortoiliac atherosclerosis: a preliminary study. *Folia Morphol (Warsz)* 67:78–83, 2008
15. Khurma V, et al: A pilot study of subclinical coronary atherosclerosis in systemic sclerosis: coronary artery calcification in cases and controls. *Arthritis Rheum* 59:591–597, 2008
16. Motoyama S, et al: Atherosclerotic plaque characterization by 0.5-mm-slice multislice computed tomographic imaging. *Circ J* 71:363–366, 2007
17. Paik DS, Beaulieu CF, Jeffrey RB, Rubin GD, Napel S: Automated flight path planning for virtual endoscopy. *Med Phys* 25:629–637, 1998
18. Raman R, Raman B, Napel S, Rubin GD: Improved speed of bone removal in computed tomographic angiography using automated targeted morphological separation: method and evaluation in computed tomographic angiography of lower extremity occlusive disease. *J Comput Assist Tomogr* 32:485–491, 2008
19. Schuirmann DJ: A comparison of the two one-sided tests procedure and the power approach for assessing the equivalence of average bioavailability. *J Pharmacokinetic Biopharm* 15:657–680, 1987
20. Adame IM, van der Geest RJ, Bluemke DA, Lima JA, Reiber JH, Lelieveldt BP: Automatic vessel wall contour detection and quantification of wall thickness in in-vivo MR images of the human aorta. *J Magn Reson Imaging* 24:595–602, 2006
21. Adame IM, de Koning PJ, Lelieveldt BP, Wasserman BA, Reiber JH, van der Geest RJ: An integrated automated analysis method for quantifying vessel stenosis and plaque burden from carotid MRI images: combined postprocessing of MRA and vessel wall MR. *Stroke* 37:2162–2164, 2006
22. Auer M, Stollberger R, Regitnig P, Ebner F, Holzzapfel GA: 3-D reconstruction of tissue components for atherosclerotic human arteries using ex vivo high-resolution MRI. *IEEE Trans Med Imaging* 25:345–357, 2006
23. Cardinal MH, Meunier J, Soulez G, Maurice RL, Therasse E, Cloutier G: Intravascular ultrasound image segmentation: a three-dimensional fast-marching method based on gray level distributions. *IEEE Trans Med Imaging* 25:590–601, 2006
24. Clarke SE, Beletsky V, Hammond RR, Hegele RA, Rutt BK: Validation of automatically classified magnetic resonance images for carotid plaque compositional analysis. *Stroke* 37:93–97, 2006
25. Desai MY, Lai S, Barmet C, Weiss RG, Stuber M: Reproducibility of 3D free-breathing magnetic resonance coronary vessel wall imaging. *Eur Heart J* 26:2320–2324, 2005
26. Dwyer JH, Sun P, Kwong-Fu H, Dwyer KM, Selzer RH: Automated intima-media thickness: the Los Angeles Atherosclerosis Study. *Ultrasound Med Biol* 24:981–987, 1998
27. Fenster A, Blake C, Gyacskov I, Landry A, Spence JD: 3D ultrasound analysis of carotid plaque volume and surface morphology. *Ultrasonics* 44(Suppl 1):e153–e157, 2006
28. Giannoglou GD, et al: A novel active contour model for fully automated segmentation of intravascular ultrasound images: in vivo validation in human coronary arteries. *Comput Biol Med* 37:1292–1302, 2007
29. Hagenaaers T, et al: Progression of atherosclerosis at one-year follow-up seen with volumetric intravascular ultrasound in femoropopliteal arteries. *Am J Cardiol* 85:226–231, 2000
30. Haley AP, et al: Carotid artery intima-media thickness and cognition in cardiovascular disease. *Int J Cardiol* 121:148–154, 2007
31. Heuten H, Goovaerts I, Ennekens G, Vrints C: Carotid artery intima-media thickness is associated with coronary artery disease. *Acta Cardiol* 63:309–313, 2008
32. Kaneda H, Kataoka T, Ako J, Honda Y, Yock PG, Fitzgerald PJ: Coronary risk factors and coronary atheroma burden at severely narrowing segments. *Int J Cardiol* 124:124–126, 2008
33. Kara S, Dirgenali F: Detection of atherosclerosis using autoregressive modelling and principles component analysis to carotid artery Doppler signals. *Biomed Mater Eng* 16:269–277, 2006
34. Kerwin W, et al: Magnetic resonance imaging of carotid atherosclerosis: plaque analysis. *Top Magn Reson Imaging* 18:371–378, 2007
35. King M, Giger ML, Suzuki K, Pan X: Feature-based characterization of motion-contaminated calcified plaques in cardiac multidetector CT. *Med Phys* 34:4860–4875, 2007
36. King M, et al: Computerized assessment of motion-contaminated calcified plaques in cardiac multidetector CT. *Med Phys* 34:4876–4889, 2007
37. Lilledahl MB, Haugen OA, de Lange Davies C, Svaasand LO: Characterization of vulnerable plaques by multiphoton microscopy. *J Biomed Opt* 12:044005, 2007
38. Mougiakakou SG, Golemati S, Gousias I, Nicolaides AN, Nikita KS: Computer-aided diagnosis of carotid atherosclerosis based on ultrasound image statistics, laws' texture and neural networks. *Ultrasound Med Biol* 33:26–36, 2007
39. Nadkarni SK, Bilenca A, Bouma BE, Tearney GJ: Measurement of fibrous cap thickness in atherosclerotic plaques by spatiotemporal analysis of laser speckle images. *J Biomed Opt* 11:021006, 2006
40. Naqvi TZ: Ultrasound vascular screening for cardiovascular risk assessment. Why, when and how? *Minerva Cardioangiol* 54:53–67, 2006
41. Ozkan U, Oguzkurt L, Tercan F, Nursal TZ: The prevalence and clinical predictors of incidental atherosclerotic renal artery stenosis. *Eur J Radiol* 69:550–554, 2007
42. Preik M, Lauer T, Heiss C, Tabery S, Strauer BE, Kelm M: Automated ultrasonic measurement of human arteries for the determination of endothelial function. *Ultraschall Med* 21:195–198, 2000
43. Seabra JC, Sanches JM, Pedro LM, Fernandes JF: Carotid plaque 3D compound imaging and echo-morphology analysis: a Bayesian approach. *Conf Proc IEEE Eng Med Biol Soc* 2007:763–766, 2007
44. Steen H, et al: High-resolution three-dimensional aortic magnetic resonance angiography and quantitative vessel wall characterization of different atherosclerotic stages in a rabbit model. *Invest Radiol* 42:614–621, 2007
45. Stoitsis J, Tsiaparas N, Golemati S, Nikita KS: Characterization of carotid atherosclerotic plaques using frequency-based texture analysis and bootstrap. *Conf Proc IEEE Eng Med Biol Soc* 1:2392–2395, 2006

46. van der Meer FJ, Faber DJ, Baraznji Sassoon DM, Aalders MC, Pasterkamp G, van Leeuwen TG: Localized measurement of optical attenuation coefficients of atherosclerotic plaque constituents by quantitative optical coherence tomography. *IEEE Trans Med Imaging* 24:1369–1376, 2005
47. Jadhav UM, Kadam NN: Non-invasive assessment of arterial stiffness by pulse-wave velocity correlates with endothelial dysfunction. *Indian Heart J* 57:226–232, 2005
48. Shum J, et al: Semiautomatic vessel wall detection and quantification of wall thickness in computed tomography images of human abdominal aortic aneurysms. *Med Phys* 37:638–648, 2010
49. Raman R, Napel S, Beaulieu CF, Bain ES, Jeffrey Jr, RB, Rubin GD: Automated generation of curved planar reformations from volume data: method and evaluation. *Radiology* 223:275–280, 2002